Biosensors and Bioelectronics 212 (2022) 114390

Contents lists available at ScienceDirect

Biosensors and Bioelectronics

journal homepage: www.elsevier.com/locate/bios

A microfluidic chemiluminescence biosensor based on multiple signal amplification for rapid and sensitive detection of *E. coli* O157:H7

Dongli Sun [a], Tingting Fan [a], Feng Liu [a], Fangxiu Wang [c], Dan Gao [a,*], Jin-Ming Lin [b,**]

[a] The State Key Laboratory of Chemical Oncogenomics, Key Laboratory of Chemical Biology, Tsinghua Shenzhen International Graduate School, Tsinghua University, Shenzhen, 518055, China
[b] Department of Chemistry, Beijing Key Laboratory of Microanalytical Methods and Instrumentation, The Key Laboratory of Bioorganic Phosphorus Chemistry & Chemical Biology, Tsinghua University, Beijing, 100084, China
[c] Shenzhen Lvshiyuan Biotechnology Co. Ltd, Shenzhen, 518120, China

ARTICLE INFO

Keywords:
Microfluidic chip
Catalytic hairpin assembly
Chemiluminescence
Au NPs
E. coli O157:H7

ABSTRACT

E. coli O157:H7 has become a crucial foodborne pathogen with certain morbidity and mortality. However, the available methods still face the significant challenges including the improvement of detection specificity and sensitivity for real sample analysis. Herein, a microfluidic chemiluminescence biosensor based on a multiple signal amplification strategy was developed for rapid and ultrasensitive detection of *E. coli* O157:H7. The microfluidic device was consisted of an upstream snake-shape mixing channel and a downstream ship-shape microcavity with micropillar array for high efficient mixing of CL reagents, sufficient CHA amplification reaction and CL reaction. The multiple signal amplification was achieved by bacteria competitively bind to trigger catalytic hairpin assembly (CHA) and HRP-Au NPs catalyzed CL reaction. Based on the platform, the detection of target bacteria is converted to the detection of nucleic acid with a limit detection down to 130 CFU/mL, which is better or comparable to previously reported biosensors. Moreover, the whole analysis time was about 1.5 h with only 10 μL of sample. The biosensor exhibited an excellent recovery rate ranged from 90.0% to 110.0% and good selectivity to the target bacteria. Overall, this developed biosensor is a promising tool for ultrahigh sensitive and rapid detection of foodborne pathogens.

1. Introduction

Shiga toxin-producing *Escherichia coli* O157: H7 (*E. coli* O157:H7), as an important food-borne pathogen, has caused 63,000 hemorrhagic colitis cases annually in the United States and 2.8 million global cases according to 10 out of 14 world health organization subregions (Ameer et al., 2021). One of the key strategies to prevent and control *E. coli* O157: H7 is effective and rapid detection of *E. coli* O157: H7 since its infectious dose is estimated to be as low as 10 to 100 cells. To date, the gold standard for this pathogen detection basically relies on culture plating, which is time-consuming and laborious for its complicated manipulation such as enrichment, purification and cell plating (Amiri et al., 2018). Alternately, Enzyme-linked immune-sorbent assay (ELISA) and polymerase chain reaction (PCR) were regarded as rapid methods for *E. coli* O157: H7 detection. However, the ELISA (Guo et al., 2016; Shan et al., 2016; Zeinhom et al., 2018) is less sensitive due to low efficiency for a solid−liquid reaction, and susceptible to false positives due to cross contamination. Although the PCR had the ability to improve detection sensitivity and specificity, it requires complex sample preparation including gene extraction, resulting the extension of the detection time (Park et al., 2021). Therefore, there is an urgent need to develop new methods for simple, rapid and sensitive detection of *E. coli* O157: H7.

In recent years, microfluidics has attracted an increasing attention in the detection of food-borne pathogens (Jiang et al., 2021; Xue et al., 2021; Yu et al., 2021), due to its distinct advantages, such as less reagent consumption, fast reaction, automatic operation, miniaturization, etc. Majority of detection technologies, such as colorimetric (Zheng et al., 2019), fluorescence (S. Fang et al., 2021b), surface-enhanced Raman scattering (Wang et al., 2017), surface plasmon resonance (Puiu and Bala, 2020), and electrochemical (Y. Li et al., 2020b) impedimetric (Sharif et al., 2019) combined with immunological (Xue et al., 2021) or

* Corresponding author.
** Corresponding author.
E-mail addresses: gao.dan@sz.tsinghua.edu.cn (D. Gao), jmlin@mail.tsinghua.edu.cn (J.-M. Lin).

https://doi.org/10.1016/j.bios.2022.114390
Received 15 January 2022; Received in revised form 4 May 2022; Accepted 15 May 2022
Available online 17 May 2022

molecular biological assays (Sharif et al., 2019) have been integrated on the microfluidic devices for pathogens detection. However, these methods still face the challenges of insufficient sensitivity, requiring complicated and tedious sample pretreatment and enrichment procedures (Azinheiro et al., 2020; Park et al., 2021; Wang et al., 2017; R. Zhou et al., 2021b; Qi et al., 2021), which greatly hinder their further practical applications. Hence, developing new sensing methods with high sensitivity and specificity for rapid detection of *E. coli* O157: H7 still remains urgent requirement.

Comparatively, chemiluminescence (CL) relies on illumination produced by chemical reactions of trace analyst, which can be exempted from the excitation light source and therefore avoid interference from light scattering (Bagheri et al., 2021). In addition, CL possesses several superior characteristics, such as wide calibration ranges, simple instrumentation and easy miniaturization, offering a great potential for sensitive and rapid determination of pathogenic microorganisms (Gu et al., 2019; Yang et al., 2019). Classically, luminol-based CL reaction coupled with hydrogen peroxide (H_2O_2) and other oxidations is the main illuminated medium because of its low cost and high sensibility (Dai et al., 2020). However, the CL signal intensity of the system still not strong enough to fulfill the requirement for trace substance or micro-organisms detection. Recently, various enzyme-free amplification strategies have been exploited to improve the detection sensitivity, like rolling circle amplification (RCA) (Y. Li et al., 2020b), hybridization chain reaction (HCR) (Liu et al., 2020), DNA walker (J. Fang et al., 2021a), catalytic hairpin assembly (CHA) (Luo et al., 2020) and so on. Among them, the CHA is a toehold-mediated strand displacement reaction driven by the free energy of base pair formation, which possesses significant advantages, such as negligible background, excellent property of amplification ability, high catalytic efficiency. Therefore, it is widely used as a sensitive sensor combined with specific aptamer for biomolecules and bacterium detection (Ye et al., 2021; Zou et al., 2021). In addition, the gold nanoparticles (Au NPs) are ideal materials as the bridge to connect CHA cycling circuit and CL reaction, since they have high specific surface area and great affinity, which can be easily modified with sulfydryl nucleic acid and horseradish peroxidase (HRP) through Au–S bond for CL reaction (Liu et al., 2016; Zhao et al., 2021). To sum up, the combination of CHA signal amplification with Au NPs-HRP catalytic CL amplification would provide a significant opportunity for high sensitive and rapid detection of food-borne pathogens.

In this work, a novel microfluidic chemiluminescence (MCL) biosensor with a multiple signal amplification was developed for rapid and sensitive detection of *E. coli* O157:H7. Briefly, a microfluidic chip composed of two functional units. An upstream snake-shape mixing unit was used for efficient mixing of luminol and H_2O_2, whereas the downstream ship-shape microcavity part with micropillar array was designed for sufficient modifying the biomolecules and further CHA amplification reaction and CL detection. For the multiple signal amplification, a complementary nucleic acid DNA chain (S) is designed to target *E. coli* O157:H7 aptamer (Apt-E), and trigger two hairpin probes (H1 and H2) spontaneous assembly. H1 was firstly modified in the microcavity area of the microchannel, whereas H2 and HRP were simultaneously immobilized on the surface of Au NPs. In the presence of the target bacteria, it can competitively bind to Apt-E to release S, and the released S triggers enzyme-free CHA amplification between H1 and H2 to form H1/H2 duplexes. As a result, Au NPs-HRP is finally fixed on the microchannel to catalyze CL reaction between luminol and H_2O_2. Hence, the detection of bacteria is converted to the detection of nucleic acid. Our developed MCL biosensor exhibited ultra-sensitive and specificity, simple operation and minimum sample consumption for food-pathogen detection, and is a promising technique for further clinical applications.

2. Materials and methods

2.1. Design of CHA cycling circuit

The CHA cycling circuit concludes three DNA strands: S chain which can conjugate with Apt-E through complementary base pairing, and two hairpin oligonucleotides (H1, H2) which can be triggered by S. The sequences of Apt-E and S were referred to the previously reported literature (T. Li et al., 2020a). In order to obtain the optimal H1 and H2, three kinds of H1 (H1-1, H1-2, H1-3) with increasing base numbers in 'toehold' segment and three kinds of H2 (H2-1, H2-2, H2-3) with different base numbers in 'toehold' segment and 'stem' segment were designed. Then the optimal H1 and H2 were linked with 9 thymines and respectively modified by biotin and thiol (-SH) at 5' end. Their sequences are listed in Table S1. The secondary structures of all hairpins were predicted by NUPACK software package (http://www.nupack.org/). Finally, all DNA probes were annealed, and their performance were evaluated by native polyacrylamide gel electrophoresis (native--PAGE) as described in Supporting Information.

2.2. Design, fabrication and modification of microfluidic device

A microfluidic chip was firstly developed as the rapid detection platform to construct the MCL biosensor. The microfluidic chip which comprised an upstream snake-shape mixing channel for efficient mixing of luminol and H_2O_2 and a downstream ship-shape microcavity with micropillar array for sufficient modifying the H1 and further CHA and CL reaction. In addition, inlet 1 was connected with microcavity to inject surface modification reagents, samples, and CHA cycling circuit probes. Inlet 2 and inlet 3 were used for the injection of luminol and H_2O_2 to the mixing channel. In detail, the mixing channel was designed with a width of 200 μm and a total length of 20 cm, and the ship-shape microcavity had a width of 3 mm and a length of 16 mm, while the micropillars had a diameter of 200 μm and the center distance between two micropillars was 400 μm. And the depth of all channels was 150 μm. This microfluidic chip was fabricated using standard soft lithography and replica molding techniques (Chen et al., 2018), and detailed process was described in Supplementary Information. Surface modification and biotin-H1 immobilization were performed according to the method displayed in the reported reference (M. Zhou et al., 2021a), and detailly presented in Supporting Information.

2.3. Preparation of H2–Au NPs-HRP

Au NPs were prepared by using a modified Turkevich method (Li et al., 2016) with details shown in Supporting Information. Then, H2–Au NPs-HRP was synthesized using a modified method according to the literature (Zhao et al., 2021) which was mentioned in Supporting Information. The size of Au NPs and H2–Au NPs-HRP were charactered by the TEM images by Tecnai G2 spirit TEM system (FEI Co., Ltd., Hillsboro, USA). The concentration of Au NPs was measured by the absorbance at 520 nm ($\varepsilon = 2.7 \times 10^8$ L mol^{-1} cm^{-1}). To measure the changes between Au NPs and H2–Au NPs-HRP, the zeta potentials and dynamic light scattering (DLS) were further characterized by Zetasizer system (Malvern Nano ZS, UK). The absorbance at 420 nm was measured to verify whether the HRP was successfully modified on Au NPs using Ultraviolet–visible (UV–vis) absorption spectrometry (Agilent Cary 100 UV–vis absorption spectrometer, Palo Alto, USA). In order to confirm the HS-H2 was also modified on Au NPs, the FAM labeled HS-H2 was modified on Au NPs, and then the emission spectrum was measured under the excitation wavelength of 490 nm before and after modification. Fluorescence spectrum were carried out in a 96-well assay plate (Costar, Washington, DC, USA) using a microplate reader (Tecan infinite M1000 Pro, Männedorf, Switzerland).

2.4. Detection of E. coli O157: H7 by the MCL biosensor

To investigate the feasibility of this MCL biosensor by assembling the microfluidic chip, syringe pump with ultraweak luminescence system (Fig. S1), a certain concentration of *E. coli* O157: H7 standard solution was tested. The bacteria were firstly cultured according to the method described elsewhere, and a calibration curve between the optical density at 600 nm (OD_{600}) and concentration of *E. coli* O157: H7 was measured using an UV-1800 spectrophotometer. These detailed experimental procedures were described in Supporting Information. Prior to detection of target bacteria on chip, 1 μL of S (10 μM) and 1.5 μL of Apt-E (10 μM) were mixed with 17.5 μL of Tirs-HCl buffer (10 mM). The mixture was annealed to form the 500 nM S/Apt-E duplex. 10 μL of 10^8 CFU/mL bacteria sample in 10 mM Tri-HCl buffer, 1 μL of 500 nM S/Apt-E duplex and 2 μL of H2–Au NPs-HRP were then simultaneously injected into the downstream ship-shape microcavity through inlet 1 and incubated 1 h to carry out CHA cycling circuit followed by washing up the unbound materials. Subsequently, 6.5 μL of luminol and 6.5 μL of H_2O_2 were simultaneously injected into the upstream snake-shape mixing channel through inlet 2 and 3 at the flow rate of 10 μL/min, which were catalyzed by the Au NPs-HRP immobilized on downstream microcavity generated from the above CHA reaction to produce CL signals. The CL signals were immediately monitored by Ultra Weak Chemiluminescence Analyzer (BPCL-2-TGC, Guangzhou Microphotonics Technology Co., Ltd, Guangzhou, China) within 15 min. For the control experiments without the present of bacteria or CHA related reagents, the CL signals were also determined on the MCL platform.

The spiked milk samples were used as the real samples, and preparation process was shown as follows. Skim milk was purchased from supermarket and sterilized at 121 °C for 20 min. Next, 100 μL 2×10^6 CFU/mL *E. coli* O157:H7 in buffer was added into 900 μL sterilized milk to prepare spike milk sample. Then, the previous sample was diluted to final concentration of 2×10^4 CFU/mL and 2×10^3 CFU/mL. Finally, the above all samples were detected by MCL biosensor.

3. Results and discussion

3.1. Overall strategy for E. coli O157: H7 detection

In this work, a microfluidic chemiluminescence (MCL) biosensor based on multiple amplification strategy through CHA and HRP-AuNPs catalytic luminol-H_2O_2 CL system was developed for rapid and highly

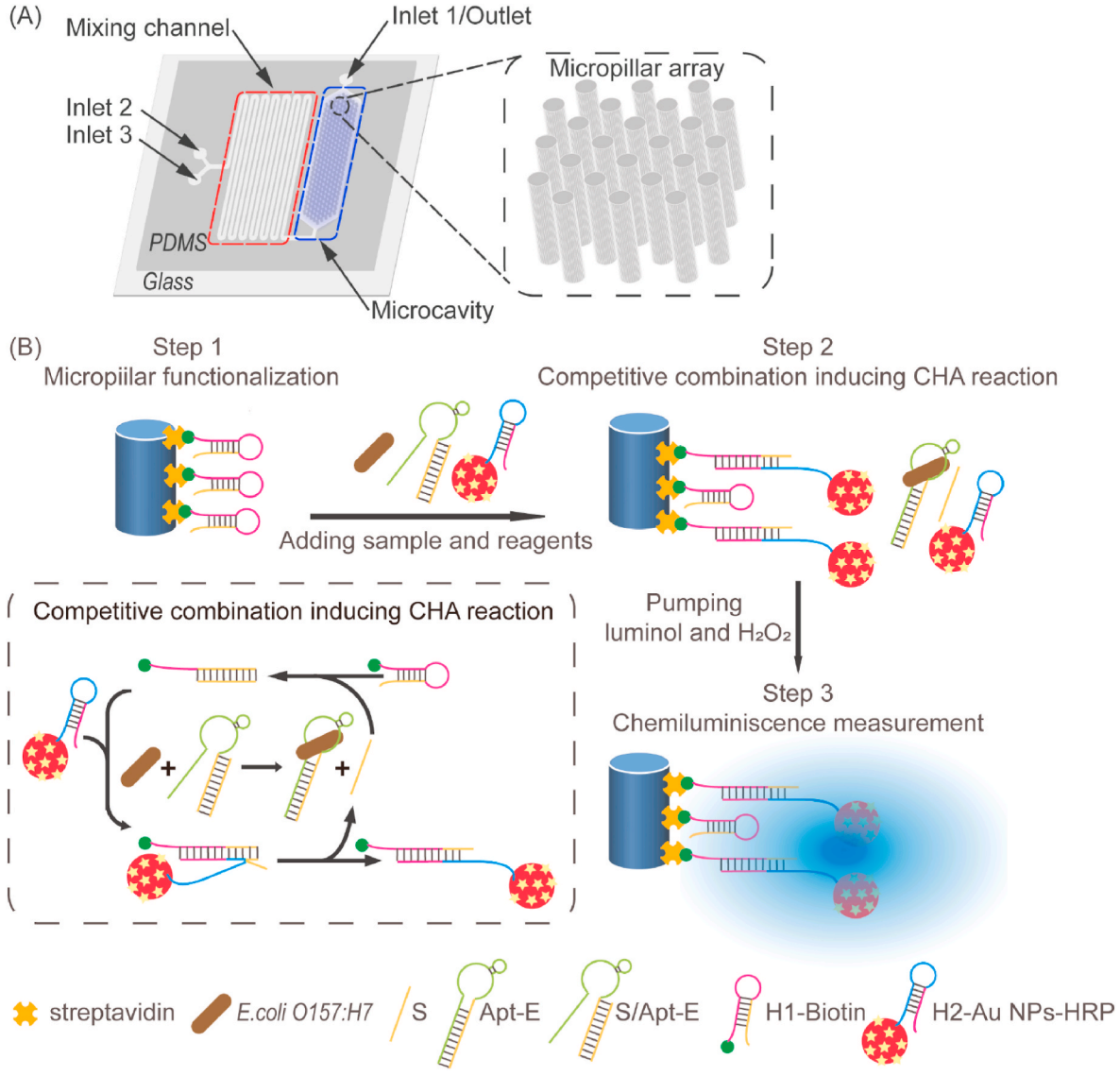

Fig. 1. Schematic illustration of the microfluidic chemiluminescence (MCL) biosensor based on multiple signal amplification strategy for detection of *E. coli* O157: H7. (A) Overall design diagram of the microfluidic chip. (B) The principle diagram of the multiple signal amplification strategy.

sensitive detection of *E. coli* O157:H7 (Fig. 1A). The microfluidic chip contained an upstream snake-shape mixing channel for efficient mixing of luminol and H_2O_2, and a downstream ship-shape microcavity with a micropillar array for sufficient immobilization of H1, performing further CHA cycling circuit and CL reaction. A photo of the microfluidic device was shown in Fig. S2. The detection procedures for *E. coli* O157: H7 were shown in Fig. 1B. Bacteria and regents were firstly injected into the downstream microcavity through inlet 1 to form CHA cycling. After washing the unbound materials with Tris-HCl buffer, the luminol and H_2O_2 were injected into upstream mixing channel through inlet 2 and 3, respectively. And they were catalyzed by the immobilized Au NPs-HRP generated from CHA reaction to produce CL signals which were simultaneously monitored by the ultra-weak luminescence Analyzer.

The multiple amplification strategy was shown in the dashed box of Fig. 1B. For CHA amplification reaction, a pair of hairpins (H1 and H2) were designed which do not initially interact with each other. The initiation sequence S firstly forces the H1 to open hairpin structure and forms S/H1 intermediate, while the previously-blocked domain of H1 is unblocked and then combines with H2 to produce a more stable H1/H2 duplex along with the release of S. The released S continuously catalyzes hairpins interaction without being consumed, enabling signal amplification. To specific detection of *E. coli* O157:H7 on chip, S was conjugated with the specific aptamer of the *E. coli* O157: H7 (Apt-E) through complementary base pairing, and H1 was immobilized in the downstream microcavity of the chip, whereas H2 and HRP were co-modified on the surface of Au NPs. In the presence of *E. coli* O157:H7, the bacteria can competitively bind to the Apt-E to replace S. The released S could further trigger CHA reaction between H1 and H2, and yield a large number of H1/H2 double strands, together with Au NPs-HRP immobilized in the downstream microcavity of the chip to catalyze the CL reaction between luminal and H_2O_2. In the absence of the *E. coli* O157:H7, the S will still conjugate with Apt-E and not trigger the CHA cycling circuit even with the existence of H1 and H2 in the solution.

3.2. Evaluation of CHA performance

Before the on-chip assay, native-PAGE experiments were conducted to obtain the optimal hairpin oligos for CHA cycling circuit. Three kinds of H1 (H1-1, H1-2, H1-3) were firstly designed, and their secondary structures were predicted by NUPACK software displayed in Fig. S3. As shown in Fig. S4A, each basic DNA structure including S (lane 1), H1-1 (lane 2), H1-2 (lane 3) and H1-3 (lane 4) shows a single and narrow band, indicating the successful formation of secondary structures which were in accordance with the predicted results of NUPACK software shown in Fig. S3. Lane 5~7 illustrated the results of the mixture of S with H1-1, H1-2 and H1-3 respectively, and a new brand was displayed at the top of each lane which indicated the S/H1 duplex was successfully formed. In addition, with the increasing of the base number in 'toehold' segment of H1, the brand of S/H1 duplex became brighter, which indicated that the conjugation efficiency was improved and the conjugation efficiency between S and H1-3 was the highest. The reason can be explained from two aspects. From the view of molecular structures of these H1 sequences, H1-3 has the longest 'toehold' segment (10 bases), which made the maximum number of complementary pairing bases between S and H1-3, so that the affinity between S and H1-3 is stronger than other two sequences. In terms of Gibbs free energy, H1-3 has the highest Gibbs free energy which made the lowest stability, so that H1-3 is the easiest to enclose the hairpin structure and combined with S (Fig. S3). Therefore, H1-3 is the optimal sequence which was selected for the following CHA cycling circuit.

In order to further improve the efficiency of CHA, three kinds of H2 (H2-1, H2-2, H2-3) were also designed to obtain the optimal H2, and their secondary structure were predicted by NUPACK software displayed in Fig. S3, and the results of native-PAGE was shown in Fig. S4B. H2-1, H2-2 and H2-3 in lane 1-3 showed a single and narrow band separately, which indicated the successfully formation of secondary structures which was in accordance with the predicted results of NUPACK software (Fig. S3). The upper bands in lane 4~6 containing the mixture of H1-3 with three kinds of H2 respectively showed the production of H1/H2 duplex. The band of H1/H2 duplex in lane 5 was brighter than other two lanes. The result demonstrated H1-3 and H2-2 had the highest degree of spontaneous interaction in absence of S. That's because the 'stem' segment (complementary pairs to form hairpin) of H2-2 is the least among the three sequences of H2, and the Gibbs free energy of the H2-2 is highest, leading to the lowest stability and most easily to enclose the hairpin structure (Fig. S3). So, the H2-2 is not an ideal sequence. Lane 7~9 shows the reaction results of H1-3 with three kinds of H2 triggered by S. Compared with lane 8 and 9, the band of H1/H2 duplex (the top band) in lane 7 was the brightest while the band of S/H1 (beneath the top band) was the darkest, proved the efficiency of CHA cycling circuit was the highest. That's because the toehold of H2-1 (8 bases) is longer than H2-3 (6 bases) which made the affinity between H2-1 and H1-3 stronger than that between H2-3 and H1-3. Therefore, H2-1 was finally selected for the following CHA cycling circuit.

The performance of the CHA cycling circuit among the S, optimized H1 and H2 was further demonstrated by native-PAGE. As shown in Fig. 2A, the upper band in lane 4 proved S was almost completely reacted with H1 to form the S/H1intermediate. The S and H2 were stably coexisted when H1 were not present (Lane 5). When the two hairpin oligos (H1 and H2) were mixed in absence of S, a small amount of H1/H2 hybrid duplex (the upper band in lane 6) was appeared which demonstrated a very slight level of spontaneous interaction between H1 and H2. However, once the initiator strand S is added, hybridization of the H1 and H2 probes is initiated, resulting in the formation of a great amount of stable H1/H2 duplex (the upper band in lane 6) but without the loss of S in the solution, demonstrating a high effective CHA cycling circuit. These results were consistent with the data obtained from the thermodynamic analysis of the equilibrium concentration of all strands by NUPACK software package (Fig. 2B). Assuming equal concentrations of the S, H1 and H2 probes (1 μM each), over 99 % of the H1 probe hybridized to the H2 probe to form H1/H2 hybrid complexes, and less than 1% of S/H1 and S/H2 are left. These results suggest that this CHA cycling circuit is thermodynamically feasible and highly effective.

In order to investigate the CHA reaction on Au NPS-HRP, H1 was labelled with FAM (Ex = 490 nm, Em > 500 nm). Then 20 μL 25 nM of S, 20 μL 25 nM FAM-H1 and 20 μL H2–Au NPs-HRP were mixed with 40 μL Tris-HCl buffer (10 mM Tris, 5 mM $MgCl_2$, 300 mM NaCl, pH 7.5), following incubation for 1 h at 25 °C. The groups without FAM-H1 or S were used as control. Then, the mixture was centrifugated in 14000 rpm at 4 °C for 30 min three times, and the obtained precipitate was resuspended in ultrapure water. Finally, the FL spectra intensity were monitored by microplate reader (Tecan infinite M1000 Pro, Männedorf, Switzerland) with excitation wavelength at 490 nm (Fig. 2C). Only the group containing all CHA reagents exhibited strong FL signal intensity up to 170, almost 10 times higher than the solution without S. The result revealed the high signal amplifaication of this CHA reaction, and demonstrated the feasibility of CHA on the surface of Au NPs-HRP. In order to obtain the best conditions of CHA on Au NPs-HRP. Reaction temperature (Fig. S5A) and time (Fig. S5B) of CHA on Au NPs-HRP were optimized, and results were shown in Supporting Information. The optimal reaction temperature and time of CHA on Au NPs-HRP were respectively 1 h and 25 °C respectively, which was in accordance with the reported reference (Bodulev et al., 2021).

3.3. Characterization of H2–Au NPs-HRP

Since Au NPs-based bioconjugation with a high mole ratio of HRP for signal amplification, H2–Au NPs-HRP were prepared to combine the CHA cycling circuit with CL reaction to dramatically enhance the CL signals on one platform. Firstly, the synthetic Au NPs and H2–Au NPs-HRP were characterized by the TEM images and shown in Fig. 3. The average diameter of the synthesized Au NPs was about 13 nm (Fig. 3A).

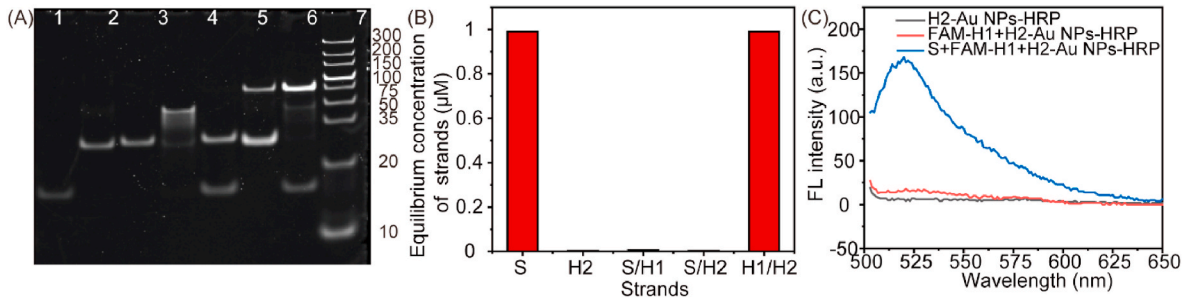

Fig. 2. Performance of hairpin probes and CHA. (A) Gel electrophoresis picture of feasibility of CHA cycling circuit, Lane 1: S; Lane 2: H1; Lane 3: H2; Lane 4: S + H1; Lane 5: S + H2; Lane 6: H1+H23; Lane 7: S + H1+H2; all final concentration of oligos for CHA reaction were 200 nM in 10 μL reaction system. (B) The results of CHA cycling circuit among the S, H1 and H2 predicted by NUPACK software, assuming equal concentrations of the S, H1 and H2 probes (1 μM each). (C) The investigation of CHA on Au NPs-HRP. The concentrations of S and FAM-H1 were both 25 nM, while initial concentration of H2 to modify on Au NPs was 0.77 μM.

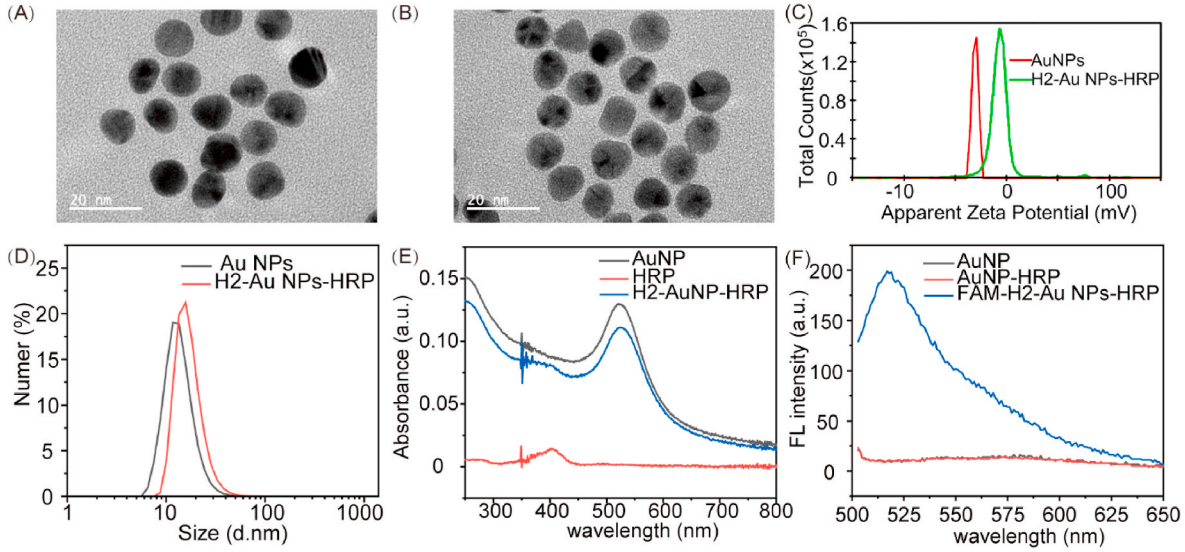

Fig. 3. Characterization of Au NPs and H2–Au NPs-HRP. The TEM images of (A) Au NPs and (B) H2–Au NPs-HRP. (C) The zeta potentials and (D) Size of Au NPs and H2–Au NPs-HRP. (E) The UV–Vis absorption spectra of Au NPs, HRP, and H2–Au NPs-HRP. (F)Fluorescence spectra of Au NPs before and after modification with HRP or both FAM-H2 and HRP.

However, the color of nanoparticles became weak after modified with H2 and HRP, and their size slightly increased (Fig. 3B). To explain this color changes, the zeta potentials was further characterized as shown in Fig. 3C, the apparent zeta potential of nano particles was increased from -20 mV to -10 mv after modified with H2 and HRP due to the coverage of the surfaces of Au NPs with H2 and HRP. This change means the conductivity of nanoparticles decrease, leading to the lighter color in TEM image in Fig. 3B. To measure the size change between AuNPs and H2–Au NPs-HRP, DLS analysis was performed, and results were shown in the curves of size distribution by number presented in Fig. 3D, The diameters of nanoparticles were slightly increased from 13.9 nm to 17.3 nm after modified with H2 and HRP, which was in accordance with the reported reference (Hong et al., 2021; Liu et al., 2017).

The Au NPs before and after modification with H2 and HRP were monitored by microplate reader. The UV–vis absorption spectra of Au NPs, HRP, and H2–Au NPs-HRP was shown in Fig. 3E. As seen from black and red curves, Au NPs gave an absorption peak at 520 nm, and HRP exhibited absorption peak at 402 nm. From the blue curve, we can see two characteristic peaks appeared at 402 nm and 520 nm, indicating the successful modification of HRP on the surface of Au NPs. The peak at 402 nm could be assigned to the characteristic peak of the hemin on HRP. To further verify the modification of H2 on the surface of Au NPs, H2 was labeled with FAM (Ex = 490 nm, Em > 500 nm), and the synthesized product of FAM-H2-Au NPs-HRP, Au NPs, and HRP were characterized by microplate reader with emission wavelength at 490 nm (Fig. 3F). As seen from black curve and red curve, Au NPS and Au NPs-HRP had no emission light, while the FAM-H2-Au NPs-HRP had a characteristic peak at 520 nm, which is originated from the emission of FAM, further confirming the successful preparation of H2–Au NPs-HRP.

3.4. Optimization of the MCL biosensor

To achieve the optimal performance for *E. coli* O157:H7 detection, several experimental conditions were investigated, including the concentration ratio of S to Apt-E, the concentration of the biotin-H1 modified in the microchannel and the injection flow rate of luminol and H_2O_2. To optimize the concentration ratio of S to Apt-E, different ratios of S to Apt-E ranging from 1:1 to 1:2 were prepared to form S/Apt-E duplex. As shown in the lanes from 3 to 7 in Fig. 4A, when S: Apt-E was lower than 1:1.5, there is no dissociative S in the solution. To further confirm the phenomenon, H1 and H2 were added into the above mixture solutions. The results were shown in lanes from 9 to 13 of Fig. 4A the amount of H1/H2 duplex was comparable to that without adding S (lanes 8,14 containing the mixture of H1 and H2) when the ratio of S to Apt-E was smaller than 1:1.5. Because the excess dissociative Apt-E will preferentially bind to *E. coli* O157:H7 to reduce the signal of the MCL biosensor, the dissociative Apt-E should be controlled as little as possible. Therefore, the optimal concentration of S: Apt-E is 1:1.5.

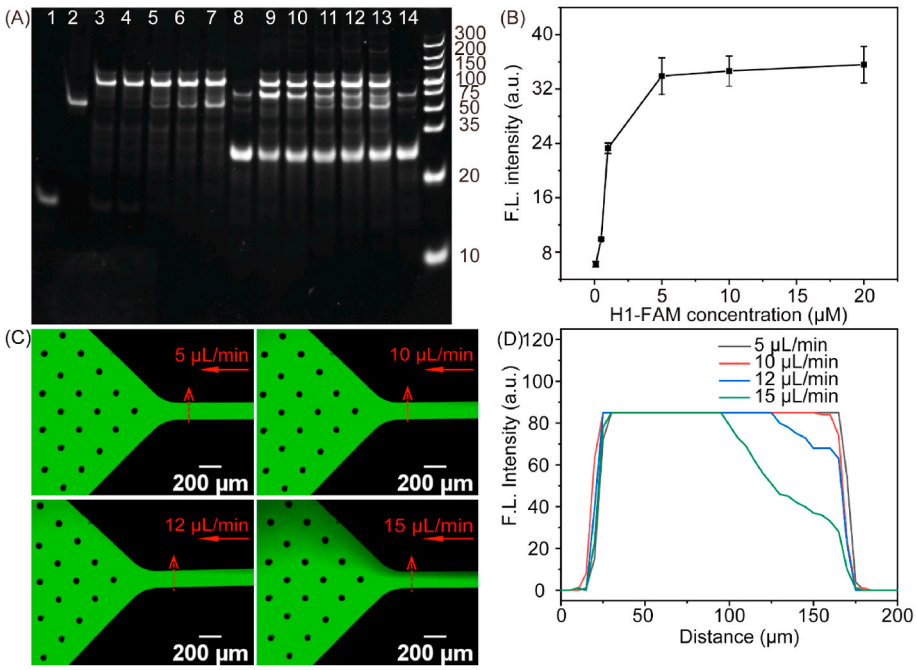

Fig. 4. Optimization of the MCL biosensor. (A)The gel electrophoresis picture of the S:Apt-E concentration ratio optimization, Lane 1: S; Lane 2: Apt-E; Lane 3: S + Apt-E (1:1); Lane 4: S + Apt-E (1:1.2); Lane 5: S + Apt-E (1:1.5); Lane 6: S + Apt-E (1:1.8); Lane 7: S + Apt-E (1:2); Lane 8: H1+H2; Lane 9: S + Apt-E (1:1)+ H1+H2; Lane 10: S + Apt-E (1:1.2)+ H1+H2; Lane 11: S + Apt-E (1:1.5)+ H1+H2; Lane 12: S + Apt-E (1:1.8)+ H1+H2; Lane 13: S + Apt-E (1:2)+ H13+H2; Lane 14: H1+H2; all final concentration of oligos for nucleic acids reaction were 200 nM in 10 μL reaction system. (B)The optimization of the concentration of bio-H1 modified on microfluidic chip. (C) The Fluorescence microscope picture of the flow rate optimization and (D) the distribution of fluorescence intensity at the junctions between the mixing channel and the ship-shape microcavity with the increasing flow rate (indicated by the red dotted line). The concentration of fluorescein sodium was 100 nM.

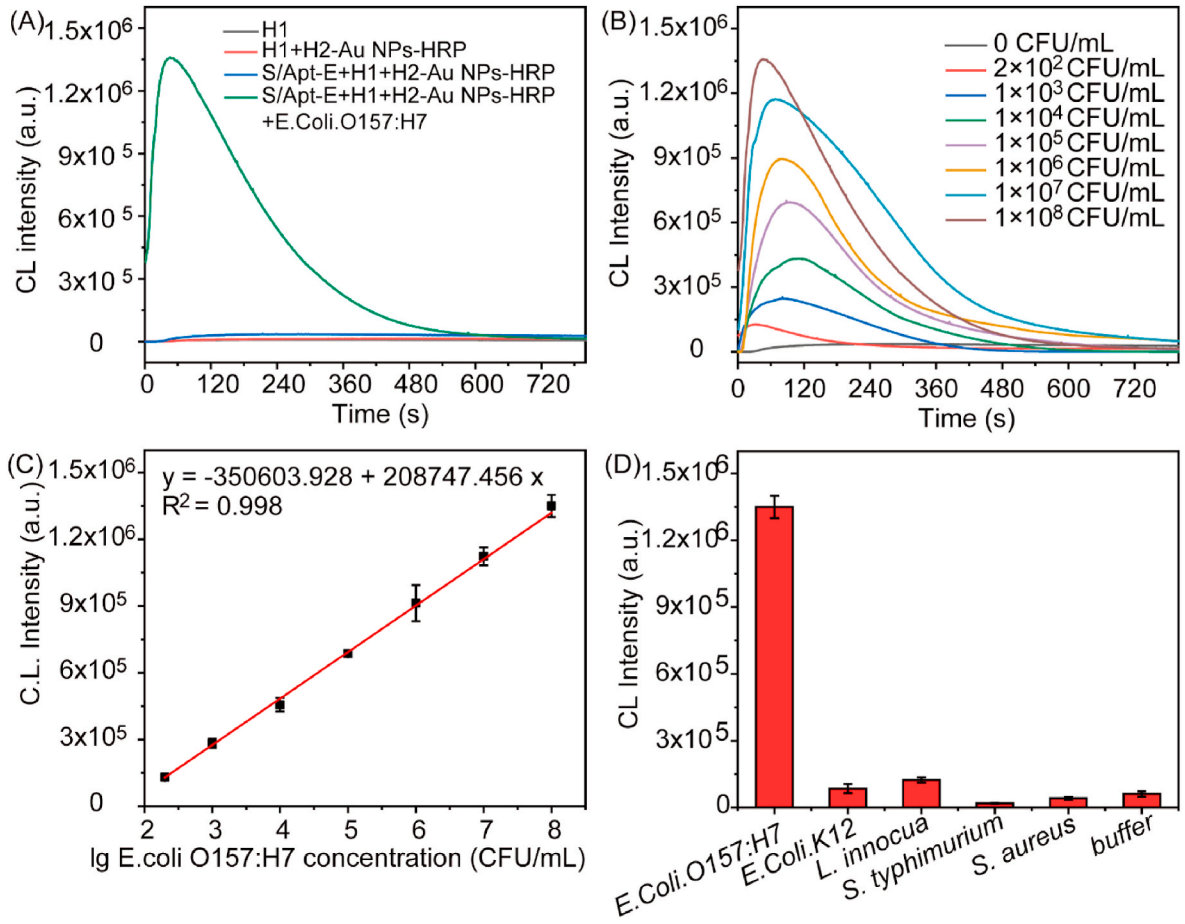

Fig. 5. The feasibility and performance of MCL biosensor based on multiple signal amplification strategy. (A) The feasibility of MCL biosensor. The final concentration of S/Apt-E was 50 nM; the initial concentration of H1 modified on chip was 5 μM; the initial concentration of H2 to modify on Au NPs was 0.77 μM; while concentration of target bacteria was 1×10^8 CFU/mL. (B) The CL spectra of the MCL biosensor for different concentration *E. coli* O157: H7 detection. (C) The calibration curve of the MCL biosensor for *E. coli* O157: H7 detection. (D) The specificity of the MCL biosensor for *E. coli* O157: H7 detection, while concentration of all bacteria was 1×10^8 CFU/mL. Data shown are averages plus and minus the standard deviation of three independent experiments.

The concentration of the biotin labeled H1 for CHA reaction should be firstly investigated to ensure the completely modification of the inner surface of the channel by H1. In order to directly evaluate the modification performance by inverted fluorescence microscope (Leica DMI 4000, Leica microsystem Co., Ltd, Shanghai, China), a biotin-labeled H1 with a fluorescein probe (FAM) was used. The detailed modification process was displayed in Supporting Information. And a fluorescence image of the modified microcavity area in the microchannel with 5 μM of the bio-H1-FAM was shown in Fig. S6. As shown in Fig. 4B, when the concentration of biotin-H1-FAM increased from 0.1 μM to 20 μM, the fluorescence signal remained nearly the same at the concentration of 5 μM, which means the saturated modification at this concentration. Therefore, we used 5 μM biotin-labeled H1 for inner surface modification in the following experiments.

Since the mixture efficiency of Luminol and H_2O_2 for CL reaction was significantly affected by the injection flow rate. A fluorescence probe, fluorescein sodium (Ex = 490 nm, Em > 510 nm) with comparable molecular weight of luminol, was used as a detectable indicator to estimate the mixing efficiency. The ultra-pure water and fluorescein sodium solution were injected into the snake-shape mixing channel from the inlet 2 and inlet 3, respectively, at a flow rate of 5, 10, 12, and 15 μL/min using a syringe pump. The distribution of fluorescence intensities at the junctions (indicated by the red dotted arrow in Fig. 4C) between the mixing channel and the ship-shape microcavity were imaged by fluorescence microscope and quantified by Image J software. As shown in Fig. 4D the fluorescence intensity with the direction of the arrow reached equilibrium when the flow rate was less than 10 μL/min, which indicated sufficient mixing at this condition. In order to ensure short analysis time, the injection flow rate of 10 μL/min was finally selected for the following experiment.

3.5. Feasibility and performance of this MCL biosensor

To further investigate the feasibility and performance of the established MCL biosensor under the optimized conditions, 1×10^8 CFU/mL *E. coli* O157:H7 spiked buffer was detected. The concentration of bacteria was obtained from the calibration curve of OD_{600} and *E. coli* O157: H7 concentration shown in Fig. S7. The samples without complete CHA reagents or target bacteria were used as control. As shown in Fig. 5A, only the sample containing bacteria and all CHA reagents exhibited strong CL signal intensity up to 1.3×10^6, almost 23 times higher than the solutions without *E. coli* O157:H7 or anyone of CHA reagents. The result revealed that the established MCL biosensor have strong response signal and high signal to noise ratio (SNR), which has the potential for *E. coli* O157:H7 detection.

The sensitivity of this biosensor was further studied. A serial concentration of bacteria ranging from 2×10^2 to 10^8 CFU/mL were detected on chip under optimal conditions to obtain the working curve referring to corresponding CL signal intensity. As shown in Fig. 5B, the CL signal intensity increased with the increasing concentration of *E. coli* O157:H7. The corresponding quantification result was obtained by plotting between the logarithm of *E. coli* O157:H7 concentration (x) and the corresponding CL peak height (y) (Fig. 5C). The fitting formula was $y = -350603.928 + 208747.456\ x$, with the $R^2 = 0.998$.

When *E. coli* O157:H7 concentration increased in the CHA cycling circuit system, more S/Apt-E was consumed because of the competitive combination between *E. coli* O157:H7 and Apt-E, while more S was dissociated from S/Apt-E to initiate the CHA cycling circuit. Because H2 and HRP were simultaneously modified on the surface of Au NPs, the more amount of H1/H2 complexes would contain higher concentration of HRP that resulted in the increasing CL signals. Each data point was obtained from three independent experiments. And then the calibration curve was obtained and shown in Fig. 5C. The fitting formula was $y = -350603.928 + 208747.456\ x$, with the $R^2 = 0.998$. The detection limit was calculated to be 130 CFU/mL based on 3-folds of the standard deviation (SD) above the blank value, which was lower than most of the reported methods (Azinheiro et al., 2020; T. Li et al., 2020a).

To verify the specificity of the MCL biosensor, five different pathogens of *E. coli* O157: H7, *E. coli* K12, *S. typhimurium, S. aureus*, and *L. innnocua* with the same concentration of 1×10^8 CFU/mL were tested. The buffer without pathogen was used as blank control. As shown in Fig. 5D, only the target *E. coli* O157:H7 had a considerable CL intensity. The interference bacteria, *E. coli* K12, *S. typhimurium, S. aureus*, and *L. innnocua* had only low and negligible CL intensity. All the above results indicated that the MCL biosensor had the analytical ability to detect *E. coli* O157: H7 in food samples. Our developed method can also be extended to other foodborne pathogens detection.

3.6. Real sample analysis

In order to evaluate the analytical reliability and application potential of our established MCL biosensor platform, three milk samples spiked with different concentrations of *E. coli* O157: H7 (2.0×10^3, 2.0×10^4, and 2.0×10^5 CFU/mL) were analyzed and three independent experiments were performed. The milk samples without spiked *E. coli* O157: H7 was used as control. The result was shown in Table 1. There were no significant differences between the results obtained by MCL biosensor and the spiked concentration of *E. coli* O157: H7. Besides, the recoveries for different concentrations of spiked samples ranged from 90.0% to 110.0%, and the average recovery rate was 101.7%. The results indicate that our developed MCL biosensor had good accuracy which has great potential for *E. coli* O157:H7 detection in real samples.

4. Conclusions

In summary, we have described a novel MCL biosensor for rapid and highly sensitive detection of *E. coli* O157:H7 based on a multiple amplification strategy through CHA and HRP-Au NPs catalytic CL reaction. Compared to the previously reported biosensors, our developed method exhibited several merits for target bacteria detection. First, due to the designed micropillar array structure and snake-shape mixing channel on chip, the efficiency of CHA and CL reaction were greatly improved. Therefore, the developed MCL biosensor was able to detect target bacteria down to 130 CFU/mL and wide dynamic range in 10 μL sample. Second, the average recovery rate of 101.7% demonstrated the excellent assay accuracy. Third, the bacteria sensing platform exhibited good selectivity to target bacteria and can realize rapid detection within 1.5 h with simple operations. Considering these advantages, this developed MCL biosensor has great application potential in food-borne pathogens detection.

CRediT authorship contribution statement

Dongli Sun: Investigation, Conceptualization, Methodology, Data curation, Formal analysis, Writing – original draft. **Tingting Fan:** Conceptualization, Methodology, Formal analysis, Writing – original draft. **Feng Liu:** Conceptualization, Methodology. **Fangxiu Wang:** Providing laboratory. **Dan Gao:** Supervision, Conceptualization, Methodology, Formal analysis, Writing – review & editing, Project administration, Funding acquisition. **Jin-Ming Lin:** Supervision, Project administration, Funding acquisition.

Table 1
Detection of *E. coli* O157: H7 by the MCL biosensor in spiked milk samples (n = 3).

Sample	Spiked concentration (CFU/mL)	Measured concentration (CFU/mL)	Recovery rate (%)
1	2.0×10^3	$(2.1 \pm 0.4) \times 10^3$	105.0
2	2.0×10^4	$(1.8 \pm 0.3) \times 10^4$	90.0
3	2.0×10^5	$(2.2 \pm 0.7) \times 10^5$	110.0

Declaration of competing interest

The authors declare that they have no known competing financial interests or personal relationships that could have appeared to influence the work reported in this paper.

Acknowledgements

This study was supported by Research and Development Program in Key Areas of Guangdong Province, P.R. China (No. 2019B020209009), Natural Science Foundation of Guangdong Province, China (No. 2020A1515010660), and Shenzhen Fundamental Research and Discipline Layout project (No. JCYJ20180508152244835).

Appendix A. Supplementary data

Supplementary data to this article can be found online at https://doi.org/10.1016/j.bios.2022.114390.

References

Ameer, M.A., Wasey, A., Salen, P., 2021. Escherichia Coli (E Coli 0157 H7). StatPearls Publishing, Treasure Island (FL), pp. 1–11 [Internet].
Amiri, M., Bezaatpour, A., Jafari, H., Boukherroub, R., Szunerits, S., 2018. Electrochemical methodologies for the detection of pathogens. ACS Sens. 3, 1069–1086.
Azinheiro, S., Kant, K., Shahbazi, M.-A., Garrido-Maestu, A., Prado, M., Dieguez, L., 2020. A smart microfluidic platform for rapid multiplexed detection of foodborne pathogens. Food Control 114, 107242.
Bagheri, N., Al Lawati, H.A.J., Hassanzadeh, J., 2021. Simultaneous determination of total phenolic acids and total flavonoids in tea and honey samples using an integrated lab on a chip device. Food Chem. 342, 128338.
Bodulev, O.L., Zhao, S., Sakharov, I.Yu, 2021. Improving the sensitivity of the miRNA assay coupled with the mismatched catalytic hairpin assembly reaction by optimization of hairpin annealing conditions. Anal. Chem. 93, 6824–6830.
Chen, Y., Gao, D., Wang, Y., Lin, S., Jiang, Y., 2018. A novel 3D breast-cancer-on-chip platform for therapeutic evaluation of drug delivery systems. Anal. Chim. Acta 1036, 97–106.
Dai, B., Yin, C., Wu, J., Li, W., Zheng, L., Lin, F., Han, X., Fu, Y., Zhang, D., Zhuang, S., 2020. A flux-adaptable pump-free microfluidics-based self-contained platform for multiplex cancer biomarker detection. Lab Chip 2, 143–153.
Fang, J., Yuan, C., Li, Junjie, Li, Junlong, Yang, T., Guo, Y., Wang, D., Xue, J., Fu, W., Xie, G., 2021a. An enzyme-powered, three-dimensional lame DNA walker. Biosens. Bioelectron. 177, 112981.
Fang, S., Song, D., Zhuo, Y., Chen, Y., Zhu, A., Long, F., 2021b. Simultaneous and sensitive determination of Escherichia coli O157:H7 and Salmonella Typhimurium using evanescent wave dual-color fluorescence aptasensor based on micro/nano size effect. Biosens. Bioelectron. 185, 113288.
Gu, Z., Fu, A., Ye, L., Kuerban, K., Wang, Y., Cao, Z., 2019. Ultrasensitive chemiluminescence biosensor for nuclease and bacterial determination based on hemin-encapsulated mesoporous silica nanoparticles. ACS Sens. 4, 2922–2929.
Guo, Q., Han, J.-J., Shan, S., Liu, D.-F., Wu, S.-S., Xiong, Y.-H., Lai, W.-H., 2016. DNA-based hybridization chain reaction and biotin–streptavidin signal amplification for sensitive detection of Escherichia coli O157:H7 through ELISA. Biosens. Bioelectron. 86, 990–995.
Hong, F., Huang, C., Wu, L., Wang, M., Chen, Y., She, Y., 2021. Highly sensitive magnetic relaxation sensing method for aflatoxin B1 detection based on Au NP-assisted triple self-assembly cascade signal amplification. Biosens. Bioelectron. 192, 113489.
Jiang, H., Sun, Z., Guo, Q., Weng, X., 2021. Microfluidic thread-based electrochemical aptasensor for rapid detection of Vibrio parahaemolyticus. Biosens. Bioelectron. 182, 113191.
Li, S., Zhang, T., Zhu, Z., Gao, N., Xu, Q.-H., 2016. Lighting up the gold nanoparticles quenched fluorescence by silver nanoparticles: a separation distance study. RSC Adv. 6, 58566–58572.
Li, T., Ou, G., Chen, X., Li, Z., Hu, R., Li, Y., Yang, Y., Liu, M., 2020a. Naked-eye based point-of-care detection of E. coli O157: H7 by a signal-amplified microfluidic aptasensor. Anal. Chim. Acta 1130, 20–28.
Li, Y., Liu, H., Huang, H., Deng, J., Fang, L., Luo, J., Zhang, S., Huang, J., Liang, W., Zheng, J., 2020b. A sensitive electrochemical strategy via multiple amplification reactions for the detection of E. coli O157: H7. Biosens. Bioelectron. 147, 111752.
Liu, S., Wang, Y., Xu, W., Leng, X., Wang, H., Guo, Y., Huang, J., 2017. A novel sandwich-type electrochemical aptasensor based on GR-3D Au and aptamer-AuNPs-HRP for sensitive detection of oxytetracycline. Biosens. Bioelectron. 88, 181–187.
Liu, Y., Chen, P., Yuan, S., Sun, B., Sun, R., Meng, X., 2020. A novel method for sensitive detection of Escherichia coli O157:H7 based on an aptamer and hybridization chain reaction. Anal. Methods 12, 3734–3740.
Liu, Y.-M., Yang, J.-J., Cao, J.-T., Zhang, J.-J., Chen, Y.-H., Ren, S.-W., 2016. An electrochemiluminescence aptasensor based on CdSe/ZnS functionalized MoS2 and enzymatic biocatalytic precipitation for sensitive detection of immunoglobulin. E. Sens. Actuators, B 232, 538–544.
Luo, F., Li, Z., Dai, G., Lu, Y., He, P., Wang, Q., 2020. Ultrasensitive biosensing pathogenic bacteria by combining aptamer-induced catalysed hairpin assembly circle amplification with microchip electrophoresis. Sens. Actuators, B 306, 127577.
Park, J., Lee, K.G., Han, D.H., Lee, J.-S., Lee, S.J., Park, J.-K., 2021. Pushbutton-activated microfluidic dropenser for droplet digital PCR. Biosens. Bioelectron. 181, 113159.
Puiu, M., Bala, C., 2020. Microfluidics-integrated biosensing platforms as emergency tools for on-site field detection of foodborne pathogens. TrAC Trends Anal. Chem. (Reference Ed.) 125, 115831.
Qi, W., Zheng, L., Wang, S., Huang, F., Liu, Y., Jiang, H., Lin, J., 2021. A microfluidic biosensor for rapid and automatic detection of Salmonella using metal-organic framework and Raspberry Pi. Biosens. Bioelectron. 178, 113020.
Shan, S., Liu, D., Guo, Q., Wu, S., Chen, R., Luo, K., Hu, L., Xiong, Y., Lai, W., 2016. Sensitive detection of Escherichia coli O157:H7 based on cascade signal amplification in ELISA. J. Dairy Sci. 99, 7025–7032.
Sharif, S., Wang, Y., Ye, Z., Wang, Z., Qiu, Q., Ying, S., Ying, Y., 2019. A novel impedimetric sensor for detecting LAMP amplicons of pathogenic DNA based on magnetic separation. Sens. Actuators, B 301, 127051.
Wang, C., Madiyar, F., Yu, C., Li, J., 2017. Detection of extremely low concentration waterborne pathogen using a multiplexing self-referencing SERS microfluidic biosensor. J. Biol. Eng. 11, 9.
Xue, L., Jin, N., Guo, R., Wang, S., Qi, W., Liu, Y., Li, Y., Lin, J., 2021. Microfluidic colorimetric biosensors based on MnO 2 nanozymes and convergence–divergence spiral micromixers for rapid and sensitive detection of Salmonella. ACS Sens. 6, 2883–2892.
Yang, R., Li, F., Zhang, W., Shen, W., Yang, D., Bian, Z., Cui, H., 2019. Chemiluminescence immunoassays for simultaneous detection of three heart disease biomarkers using magnetic carbon composites and three-dimensional microfluidic paper-based device. Anal. Chem. 91, 13006–13013.
Ye, T., Lu, J., Yuan, M., Cao, H., Yin, F., Wu, X., Hao, L., Xu, F., 2021. Toehold-mediated enzyme-free cascade signal amplification for ratiometric fluorescent detection of kanamycin. Sens. Actuators, B 340, 129939.
Yu, J., Wu, H., He, L., Tan, L., Jia, Z., Gan, N., 2021. The universal dual-mode aptasensor for simultaneous determination of different bacteria based on naked eyes and microfluidic-chip together with magnetic DNA encoded probes. Talanta 225, 122062.
Zeinhom, M.M.A., Wang, Y., Song, Y., Zhu, M.-J., Lin, Y., Du, D., 2018. A portable smart-phone device for rapid and sensitive detection of E. coli O157:H7 in Yoghurt and Egg. Biosens. Bioelectron. 99, 479–485.
Zhao, L.-Z., Fu, Y.-Z., Ren, S.-W., Cao, J.-T., Liu, Y.-M., 2021. A novel chemiluminescence imaging immunosensor for prostate specific antigen detection based on a multiple signal amplification strategy. Biosens. Bioelectron. 171, 112729.
Zheng, L., Cai, G., Wang, S., Liao, M., Li, Y., Lin, J., 2019. A microfluidic colorimetric biosensor for rapid detection of Escherichia coli O157:H7 using gold nanoparticle aggregation and smart phone imaging. Biosens. Bioelectron. 124–125, 143–149.
Zhou, M., Gao, D., Yang, Z., Zhou, C., Tan, Y., Wang, W., Jiang, Y., 2021a. Streaming-enhanced, chip-based biosensor with acoustically active, biomarker-functionalized micropillars: a case study of thrombin detection. Talanta 222, 121480.
Zhou, R., Wang, C., Huang, Y., Huang, K., Wang, Y., Xu, W., Xie, L., Ying, Y., 2021b. Label-free terahertz microfluidic biosensor for sensitive DNA detection using graphene-metasurface hybrid structures. Biosens. Bioelectron. 188, 113336.
Zou, M., Su, F., Zhang, R., Jiang, X., Xiao, H., Yan, X., Yang, C., Fan, X., Wu, G., 2021. Rapid point-of-care testing for SARS-CoV-2 virus nucleic acid detection by an isothermal and nonenzymatic Signal amplification system coupled with a lateral flow immunoassay strip. Sens. Actuators, B 342, 129899.